Short communication: Updated CRN Denudation ~~datasets~~ collections in OCTOPUS v2.3

Alexandru T. Codilean[1] and Henry Munack[1]

[1]School of Science, University of Wollongong, NSW 2522, Australia

Correspondence: Alexandru T. Codilean (codilean@uow.edu.au)

Abstract. OCTOPUS v2.3 includes ~~updated~~ updates to *CRN Denudation*~~datasets~~, adding 1,311 new river basins to the *CRN ~~International~~Global* and *CRN Australia* collections. The updates bring the total number of basins with recalculated ^{10}Be denudation rates to 5,611, and those with recalculated ^{26}Al rates to 561. To improve data relevance and usability, redundant data fields have been removed, retaining only those relevant to each collection. Additional updates include the introduction of several new data fields: the latitude of the basin centroid and the effective basin-averaged atmospheric pressure, both of which improve interoperability with online erosion rate calculators. Other new fields record the extent of present-day glaciers and their potential impact on denudation rates, as well as estimates of the percentage of quartz-bearing lithologies in each basin — providing a basis for evaluating data quality. The updated data collections can be accessed at https://octopusdata.org (last access: 01 ~~Dec 2024). The *CRN International* and *CRN Australia* data collections can also be accessed via their respective~~ Feb 2025), and have been assigned the following digital object identifiers (DOIs): 10.71747/uow-r3gk326m.28216865.v1 for *CRN Global* and 10.71747/uow-r3gk326m.28216919.v1 for *CRN Australia*.

1 Introduction

The OCTOPUS database was released in 2018 and consisted of a global compilation of cosmogenic ^{10}Be and ^{26}Al measurements from modern fluvial sediment along with optically stimulated luminescence (OSL) and thermoluminescence (TL) data from fluvial sediment archives across Australia (Codilean et al., 2018). Hosted at the University of Wollongong, the database was made accessible to the research community through an Open Geospatial Consortium (OGC)-compliant web service, ensuring standardised and seamless data sharing.

In 2022, a new version of the database (OCTOPUS v2) was released (Codilean et al., 2022), introducing significant backend improvements, an upgraded web application with enhanced functionality, and updates to existing data collections, alongside the addition of new datasets. The *CRN Denudation* collections were updated, and the fluvial luminescence data were expanded to include OSL and TL ages from aeolian and lacustrine sedimentary archives, now forming the *SahulSed* collection (Codilean et al., 2022). The new version also introduced *SahulArch*, a compilation of OSL, TL, and radiocarbon ages from archaeological records in Sahul, namely, Australia, New Guinea, and the Aru Islands, connected by formerly lower sea levels (Saktura et al., 2023). Additionally, two *partner* collections — data that is hosted on the OCTOPUS platform but is not maintained by the OCTOPUS project — were integrated: a global dataset of ^{10}Be and ^{26}Al exposure ages on glacial landforms

(https://expage.github.io; last access: 01 ~~Dec 2024~~Feb 2025), and a collection of late Quaternary non-human vertebrate fossil ages from Sahul (Peters et al., 2019, 2021). Regarding system architecture, OCTOPUS v2 introduced substantial improvements by migrating to Google Cloud Platform (GCP) with a modular design that fully leverages GCP's cloud services. Additionally, it adopted a fully relational PostgreSQL database, which organises data both hierarchically and thematically, enabling seamless
30 integration of all constituent data collections. Non-cloud-native components like GeoServer and Tomcat were containerised with Docker, ensuring a fully reproducible platform on GCP. The new platform also maintained support for integration with desktop GIS applications through OGC standards, enabling direct access to geospatial data alongside the upgraded web application. Finally, version 2 of the OCTOPUS database introduced comprehensive online documentation, including detailed information about the relational database. Additionally, a GitHub repository was created to host both the documentation and
35 source code, while supplementary materials not stored in the database were made available through a Zenodo community (see online documentation for details: https://octopus-db.github.io/documentation; last access: 01 ~~Dec 2024~~Feb 2025).

Two additional updates in 2024 introduced new data collections: the *SahulChar* collection, containing sedimentary charcoal and black carbon records from Australia, New Guinea, and New Zealand (Rehn et al., 2024), and the *Indo-Pacific Pollen (IPPD)* collection, containing palaeoecological pollen data along with site and dating information from Australia and the Indo-
40 Pacific region (Herbert et al., 2024) (both in v2.2). Additionally, *SahulSed* was expanded in v2.3 to include OSL and TL ages from coastal landforms. Versions 2.2 and 2.3 also introduced ~~updated~~ updateds to *CRN Denudation*~~datasets~~, adding 1,311 new river basins to the *CRN ~~International~~Global* and *CRN Australia* collections. Key improvements to these ~~datasets~~ include the removal of redundant fields, preserving only those relevant to each collection, and the inclusion of new fields that improve interoperability with online erosion rate calculators (Balco et al., 2008; Marrero et al., 2016; Stübner et al., 2023), and enable
45 evaluating the quality of recalculated denudation rates.

Since its launch in 2018, the OCTOPUS database has recorded nearly 2,400 unique data requests (Fig. 1), with approximately 80% of these requests focused on denudation rate data. The *CRN ~~International~~Global* and *CRN Australia* collections have become important resources for the global geoscience community, facilitating synoptic studies at both regional (e.g., Sternai et al., 2019; Delunel et al., 2020; Chen et al., 2021; Codilean et al., 2021; Whipple et al., 2023) and global scales
50 ~~(e.g., Godard and Tucker, 2021; Zondervan et al., 2023; Halsted et al., 2024)~~(e.g., Godard and Tucker, 2021; Zondervan et al., 2023; Hals~ , as originally intended. Here we describe the updated *CRN ~~International~~Global* and *CRN Australia* collections focusing on spatial data coverage, new data fields, and interoperability with online calculators.

2   The updated *CRN Denudation* ~~datasets~~collections

As described in previous publications (Codilean et al., 2018, 2022) *CRN Denudation* consists of four collections. Two of
55 these, namely *CRN ~~International~~Global* and *CRN Australia*, are officially supported by the OCTOPUS project and include recalculated ^{10}Be, and where available also ^{26}Al denudation rates, and have been assigned digital object identifiers (DOIs). The remaining two collections — *CRN Large Basins* and *CRN Denudation UOW (in preparation)* — are included solely for completeness and available at https://octopusdata.org (last access: 01 ~~Dec 2024~~Feb 2025). While they do not contain
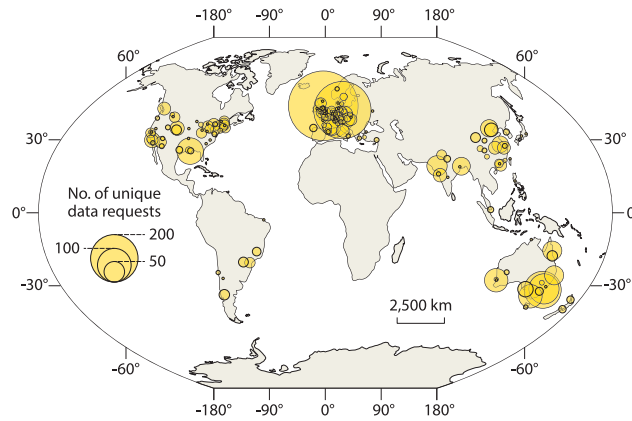
Figure 1. Geographic distribution of OCTOPUS data download requests recorded up to October 2024. Requests from outside Australia were predominantly for denudation rate data. Circle size represents the number of requests within each 25 km radius cluster.

recalculated rates, *CRN Large Basins* does include published ^{10}Be and ^{26}Al denudation rate data where available, and both collections are updated with new studies in each release as these become available.

The *CRN* ~~International~~*Global* and *CRN Australia* collections comprise 5,611 ^{10}Be and 561 ^{26}Al recalculated basin-wide denudation rates, based on data published in the peer-reviewed literature up to the start of 2024. As part of the update to version 2.3, 1,311 ^{10}Be and 163 ^{26}Al values were added (see Fig. 2). We note that the extensive ^{26}Al dataset ~~(n = 121)~~ from the recent publication by Halsted et al. (2024) has not yet been incorporated into OCTOPUS. Once included, this addition will significantly increase the number of ^{26}Al data points available in the database. Collectively, the *CRN Denudation* collections encompass data from 290 studies. A recent literature search suggests that approximately 70 publications contain relevant data not yet captured in OCTOPUS. Therefore, version 2.3 of the OCTOPUS database currently includes about 80% of all published basin-wide denudation rate studies. Of the 70 missing studies, 47 contain fewer than ten ^{10}Be basin-wide denudation rate estimates per study, with some featuring as few as two data points. Only 23 publications contain more than ten published data points per study, amounting to 363 additional ^{10}Be denudation rates, and substantially fewer ^{26}Al rates. Counting all 70 studies, version 2.3 of OCTOPUS captures roughly 90% of published data points. However, given that the 47 studies with fewer than ten data points may not be added ~~due to limited return on investment~~ to the database due to priority given to larger studies, the current version effectively captures 94% of the viable data points for inclusion in the database.

In terms of topographic characteristics, the drainage basins of *CRN* ~~International~~*Global* and *CRN Australia* span a wide range of mean elevations and slope gradients (Fig. 2a). The updated dataset has a geographical extent similar to previous versions (Codilean et al., 2018, 2022), with most data still sourced from Northern Hemisphere drainage basins (Fig. 2a). These basins primarily cluster in distinct, tectonically active regions, such as the Pacific coast of the United States, the Appalachians, the European Alps, and the Tibet-Himalaya region (Fig. 2b). Coverage is also strong in the South American Cordillera. The version 2.3 update maintains this general geographical distribution (Fig. 2c), adding new data primarily from basins along the Alpine-Himalayan and circum-Pacific orogenic belts. Importantly, new basins also fill gaps in regions such as the Atlas
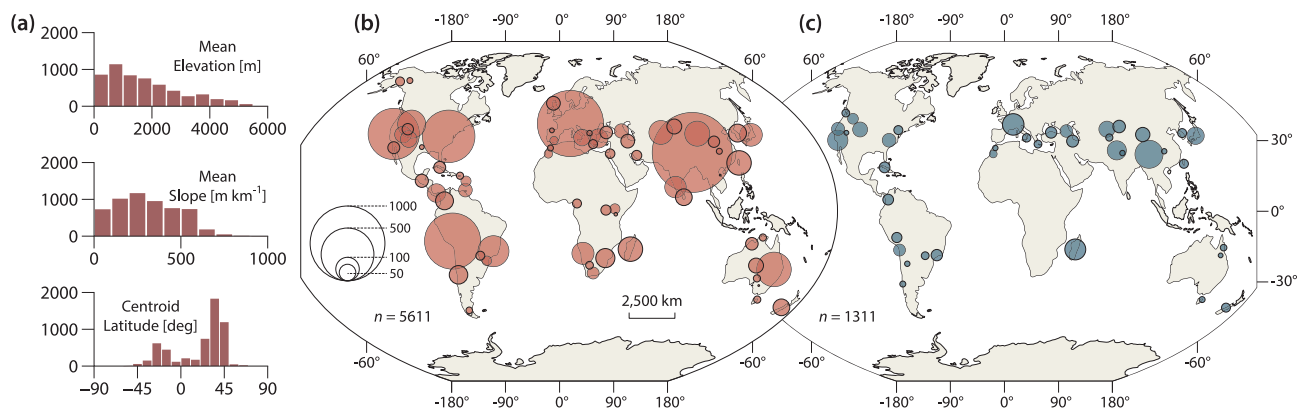
Figure 2. The updated ~~CRN International~~ *CRN Global* and *CRN Australia* data collections. (a) The distribution of mean elevation, mean slope, and centroid latitude for the 5,611 basin included in version 2.3 of the OCTOPUS database. (b) The geographic distribution of the complete data collections and (c) that of the 1,311 newly added basins in version 2.3. Circle size represents the number of requests within each 250 km radius cluster.

Mountains in North Africa, the Caucasus Mountains, and the Tian Shan. However, data from low-gradient, tectonically passive regions remain sparse, particularly in Africa. Nonetheless, the update introduces a substantial dataset from Madagascar, as well as new basins from southeastern Brazil and the Appalachians.

As with previous versions of OCTOPUS, for consistency across the *CRN Denudation* collections, published ^{10}Be and ^{26}Al concentrations $(\mathrm{atoms\,g^{-1}})$ were renormalised to the same AMS standards~~and~~, namely 07KNSTD for ^{10}Be and KNSTD for ^{26}Al (Nishiizumi, 2004; Nishiizumi et al., 2007), and basin-wide denudation rates $(\mathrm{mm\,kyr^{-1}})$ were recalculated with the open-source program CAIRN (Mudd et al., 2016). The program forward models ^{10}Be or ^{26}Al concentrations at every pixel for a given denudation rate, taking into account latitude and altitude scaling of cosmogenic nuclide production rates as well as snow, self, and topographic shielding. The obtained concentrations are averaged to predict a basin-averaged ^{10}Be or ^{26}Al concentration, and Newton's method is then used to find the denudation rate for which the predicted concentration matches the measured concentration and to derive associated uncertainties. In addition to the vector and attribute data that is stored in the PostgreSQL + PostGIS database, the *CRN* ~~International~~*Global* and *CRN Australia* collections also include seven raster data layers and a series of text files representing CAIRN configuration and input / output files (see Codilean et al., 2022, for details). These additional files are organised in "studies" — each study represents one publication — and are saved as separated zip archives with names keyed to the unique STUDYID identifier assigned to each study. The provision of these data means that users can recalculate denudation rates using updated versions of the CAIRN code, keeping the CRN ~~data~~ collections reproducible and reusable into the future.

3 Interoperability with online calculators

CRN-based Cosmogenic nuclide-based exposure ages and denudation rates require periodic recalculation as measurement standards and calculation protocols are regularly updated (Phillips et al., 2016; Schaefer et al., 2022). Online exposure age and erosion rate calculators (e.g., Balco et al., 2008; Marrero et al., 2016) play a crucial role in this process, offering platforms for dynamic and transparent data reduction. These tools harmonise disparate datasets and significantly enhance the reproducibility of cosmogenic nuclide exposure ages and erosion rates (Balco, 2020). Although the CAIRN program operates independently of existing online calculators, it has been our preferred choice for several reasons. First, CAIRN is open-source and packaged in freely available software that runs on all commonly used operating systems. Second, it is automated and designed to support reproducibility; users can publish a digital elevation model of their study area along with CRN cosmogenic ^{10}Be and ^{26}Al data and CAIRN input files, ensuring denudation rates can be replicated. Third, CAIRN is part of LSDTopoTools, a suite developed for reproducible topographic analysis (Mudd et al., 2023), allowing CRN basin-wide denudation rate calculations to seamlessly integrate with other topographic analyses within unified workflows. For computational efficiency, however, CAIRN only implements the time-independent Stone/Lal nuclide production scaling scheme (Stone, 2000)and so. This represents a significant limitation, as time-independent and time-dependent cosmogenic nuclide production scaling schemes yield results that vary systematically with denudation rate and latitude (Stübner et al., 2023). Specifically, calculated denudation rates are underestimated in slowly eroding settings and overestimated in rapidly eroding settings when a time-independent scaling scheme — that ignores geomagnetic field strength variations — is used, with differences being the largest at low latitudes (Fig. 3). Therefore, for applications where the use of more up-to-date scaling schemes is desired, users must turn to other packages (e.g., Charreau et al., 2019; Stübner et al., 2023) or make use of CAIRN's spatially averaged products for ingestion in available online calculators.

To facilitate interoperability with available online erosion rate calculators (e.g., Balco et al., 2008; Marrero et al., 2016), the *CRN International Global* and *CRN Australia* collections include two additional fields: CENTR_LAT, representing the latitude of the basin centroid, and ATM_PRESS, representing the effective basin-averaged atmospheric pressure. Both parameters are calculated by CAIRN. While the centroid latitude is straightforward, the atmospheric pressure is determined through an iterative process that identifies the pressure value best matching the spatially averaged Lal/Stone production rate (see also Mudd et al., 2016). Therefore ATM_PRESS should provide a fairly accurate single-value approximation of the spatially distributed altitude scaling factor for any given basin. It is important to note, however, that unlike the spatially distributed atmospheric pressure derived by CAIRN, which maps elevation values to atmospheric pressure using the NCEP2 climate reanalysis data (Compo et al., 2011), ATM_PRESS is not obtained from an atmospheric model. Instead, it is calculated by inverting the spatially distributed scaling model and, as such, holds no meteorological significance.

Using CENTR_LAT and ATM_PRESS with the Stone/Lal (St) scaling scheme in the Balco et al. (2008) online calculator yields ^{10}Be denudation rates that very closely match those calculated with CAIRN (Fig. 4a). For example, the median difference between values calculated with the Balco et al. (2008) calculator and those calculated with CAIRN, when using the St scaling scheme is only -0.6% (mean $= -0.3\%$) with an interquartile range (IQR) between -1.4 and 0.4%, and total range between -6.5 and 6.8%. These values are bellow the analytical uncertainties of the measured ^{10}Be concentrations recorded in the database, namely: 4.8% (median), 7.4% (mean), and $3.0 - 8.6\%$ (IQR); and well bellow the uncertainties of the calculated
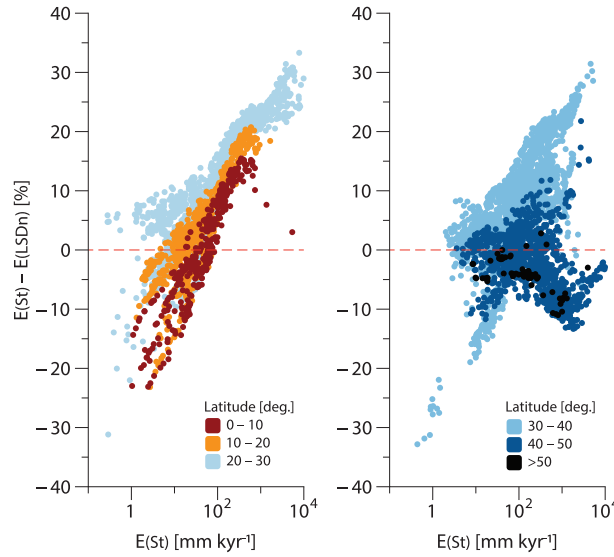
Figure 3. Comparison of ^{10}Be denudation rates calculated using the time-independent Stone/Lal (St) (Stone, 2000) scaling scheme with those calculated using the time-dependent LSDn scaling scheme (Lifton et al., 2014). Note how differences between the St and LSDn scaling schemes vary systematically with denudation rate, being the largest at low latitudes. Data points are colour-coded by latitude, with values for $< 30°$ and $> 30°$ plotted separately for clarity. Modified from Stübner et al. (2023).

denudation rates. Recalculating denudation rates with the online calculator using the ~~latitude of the basin outlet and the~~ mean
135 basin elevation instead of ~~CENTR_LAT and~~ ATM_PRESS, yields larger differences (Fig. 4b): -3.1% (median), ~~-4.5%~~ -4.4%
(mean), and ~~-5.6~~ -5.5 to -1.6% (IQR). Although these values are still within uncertainties of both ^{10}Be concentrations and
recalculated denudation rates, differences ~~between the Balco et al. (2008) calculator and CAIRN correlate with basin relief~~
~~(shown in~~ Fig. 4b ~~) with~~ correlate with basin relief, with the total range of differences being ~~-142~~ -143 to 23%. Therefore
using the effective atmospheric pressure (ATM_PRESS) instead of the mean elevation is recommended as it reliably accounts
140 for basin relief variations.

Basin relief covaries with basin area to some extent, with the largest basins in OCTOPUS also generally exhibiting the
highest relief. To test how much of the scatter in Fig. 4b is due to basin relief versus basin area, we recalculated all denudation
rates with the Balco et al. (2008) calculator using ATM_PRESS and swapping CENTR_LAT with the latitude of the basin
outlet (Fig. 5). Results are virtually identical for basins smaller than 10^4 km^2 and only become significant for basins larger
145 than 10^5 km^2 (Fig. 5b). Given that there are only 67 basins ($\sim 1\%$ of the total) in *CRN ~~International~~Global* and *CRN Australia*
that are larger than 10^5 km^2, the choice of latitude will not matter for most applications. Nevertheless, we recommend using
CENTR_LAT over the latitude of the basin outlet as the former is a better single-value approximation of the spatially distributed
latitude scaling for any given basin.

~~Since~~ Because CAIRN only implements the time-independent St scaling scheme, ~~we used RIVERSAND — a recently~~
150 ~~developed frontend to the Balco et al. (2008) calculators — to test the performance of~~ it cannot be used to test how well
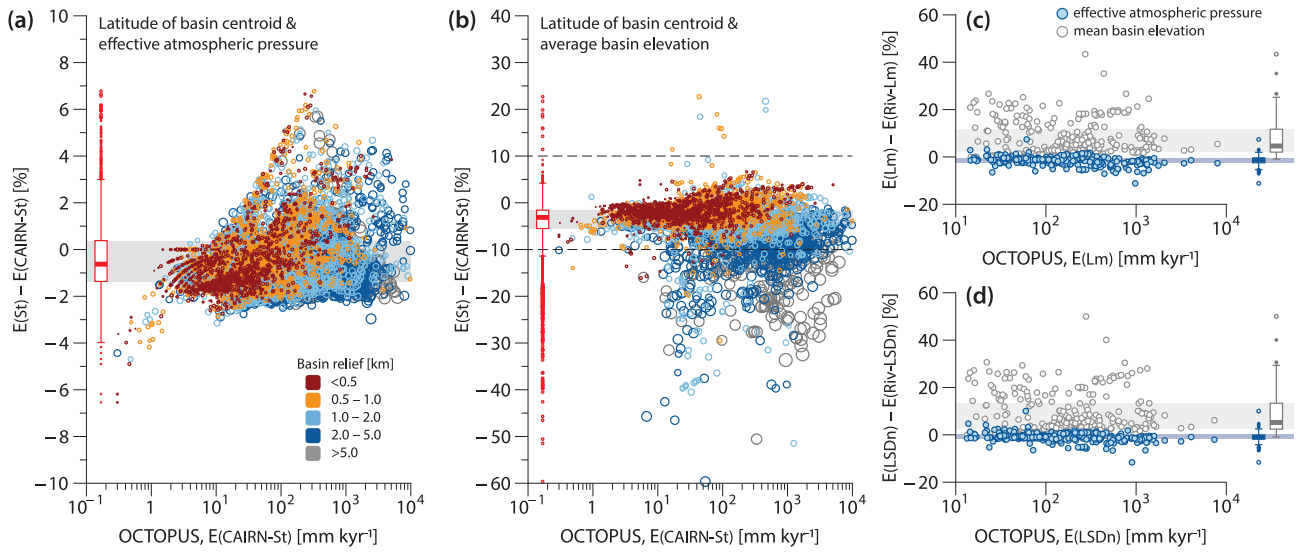
Figure 4. Comparison of [10]Be denudation rates in the OCTOPUS database with those calculated using version 3 of the Balco et al. (2008) online erosion rate calculators. (a) Percent difference between [10]Be denudation rates calculated using the St scaling scheme in the Balco et al. (2008) online calculators and those calculated with CAIRN (Mudd et al., 2016). Calculations are based on the basin centroid latitude and effective atmospheric pressure. (b) Same as (a), but ~~using~~ swapping effective atmospheric pressure with the ~~latitude of the basin outlet and~~ mean basin elevation. (c) Percent difference between [10]Be denudation rates calculated using the Lm scaling scheme in the Balco et al. (2008) online calculators and those calculated with RIVERSAND (Stübner et al., 2023) using the same Lm scaling scheme. (d) Same as (c), but using the LSDn scaling scheme. In (a) and (b), the size and colour of symbols indicate the total basin relief (km). In (c) and (d), blue symbols ~~represent~~ denote values calculated using the ~~basin centroid latitude and~~ effective atmospheric pressure, ~~while~~ whereas grey symbols ~~represent~~ indicate values ~~based on~~ derived using the ~~latitude of the basin outlet and~~ mean basin elevation. Shaded grey areas depict interquartile ranges (IQR), and the dashed horizontal lines in (b) denote the y-axis range from (a).

`CENTR_LAT` and `ATM_PRESS` perform with time-dependent scaling schemes, specifically Lm (Nishiizumi et al., 1989) and LSDn (Lifton et al., 2014), as implemented in the Balco et al. (2008) calculator. ~~RIVERSAND determines denudation rates based on~~ To rigorously calculate [10]Be denudation rates using Lm and LSDn, we used RIVERSAND — a recently developed frontend to the Balco et al. (2008) calculators that determines basin-wide denudation rates taking into account river basin hyp-
155   sometry (Stübner et al., 2023) ~~, allowing us to assess interoperability between OCTOPUS and online calculators. We~~ — and compared the resulting output to that obtained by using `CENTR_LAT` and `ATM_PRESS` with the Balco et al. (2008) calculator. For our comparison, we selected eight studies from *CRN ~~International~~Global* ~~(n = 290~~, comprising 290 [10]Be ~~datapoints) that included high relief basins (median =~~ data points. These studies included high-relief basins with a median relief of 3.6 km ~~; range between~~ and a range spanning from 0.6 ~~and~~ to 8.7 km~~) and calculated denudation rates using~~ `CENTR_LAT` ~~and~~
160   `ATM_PRESS` ~~with the Balco et al. (2008) calculator and using the digital elevation model (DEM) provided via the OCTOPUS zip archives (see Sect. 2) with RIVERSAND.~~ Differences between the two approaches are within a few percent (Fig. 4c and d) for both Lm (median = -1.3%, mean = -1.8%, IQR = -2.5 to -0.5%) and LSDn (median = -1.0%, mean = -1.2%, IQR
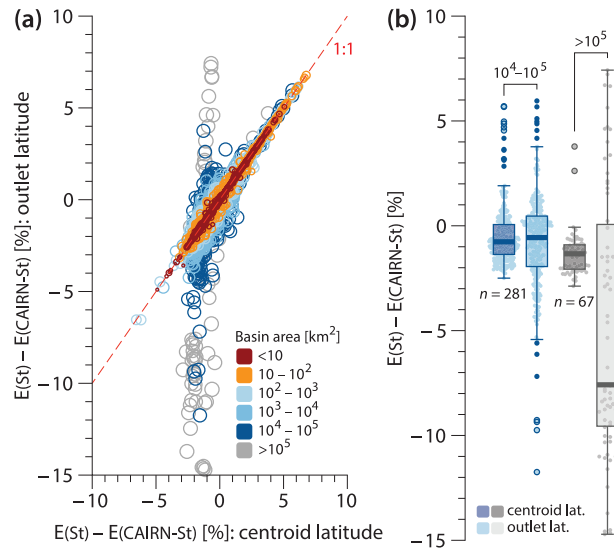
Figure 5. Comparison of ^{10}Be denudation rates calculated using basin outlet latitude versus centroid latitude. (a) Percent difference between the St scaling scheme in Balco et al. (2008) and CAIRN, comparing results using outlet latitude versus centroid latitude. Symbol size and color represent the total basin area (km^2). (b) Box-plots showing the same as in (a) for basins with areas of $10^4 - 10^5$ km^2 (blue) and $> 10^5$ km^2 (grey).

$= -1.8$ to -0.1%)~~indicating~~ . These results indicate that `CENTR_LAT` and `ATM_PRESS` are suitable approximations of basin characteristics, even in high-relief settings, and should therefore reliably reproduce denudation rates calculated using the Lm and LSDn time-dependent scaling schemes as implemented within a more rigorous, spatially distributed approach.

4 Present-day glacier coverage and inferred denudation rates

According to the Global Land Ice Measurements from Space (GLIMS) database (Raup et al., 2007), 1,014 *CRN* ~~*International*~~*Global* basins are presently glaciated. While in just over 50% of these basins ($n = 571$) present-day glacier coverage is below 5% of the total basin area, the database includes 169 basins with present-day glacier coverage over 20% and 16 basins where more than half of the basin area is covered by ice (Fig. 6). Not accounting for glacier-ice shielding will result in an overestimation of ^{10}Be-derived denudation rates (Schaefer et al., 2022). To estimate the potential extent of this overestimation, we calculated end-member ^{10}Be-derived denudation rates for the 1,014 affected *CRN* ~~*International*~~*Global* basins using present-day glacier extents from the GLIMS database. This calculation assumes that glaciated areas contribute sediment in proportion to their surface areas, with this sediment having a ^{10}Be concentration of zero. While glaciated areas may indeed contribute sediment that is depleted in cosmogenic nuclides — due to both shielding from cosmic rays and potential excavation from depth — it is improbable that glaciated areas contribute sediment strictly in proportion to their surface areas. Therefore, our glacier-corrected
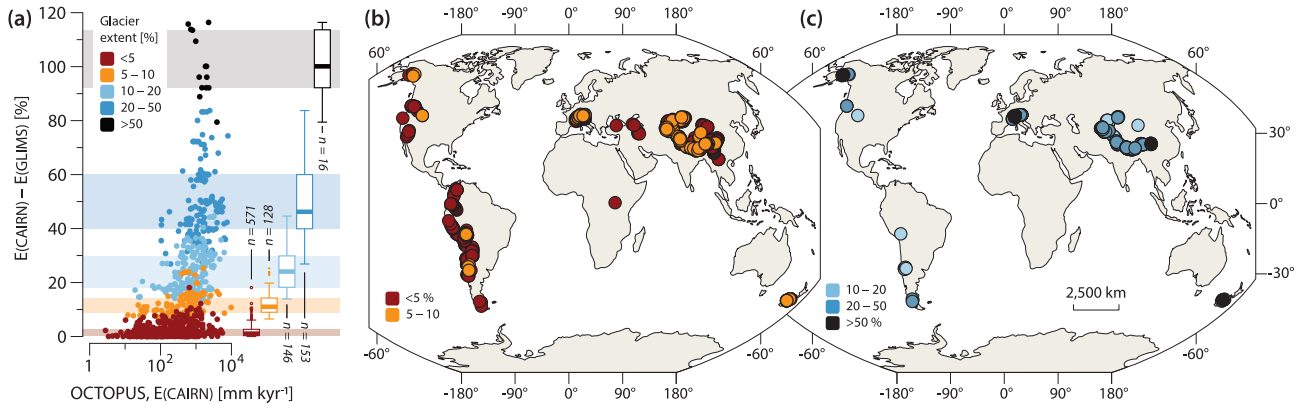
Figure 6. The influence of present-day glacier coverage on calculated ^{10}Be denudation rates. (a) Percent difference between ^{10}Be denudation rates calculated without glacier correction and those adjusted for the maximum impact of present-day glacier cover on diluting the ^{10}Be-signal exported by rivers from each affected drainage basin (see text for details). Colours indicate present-day glacier extent (%), with box plots summarising percentage difference statistics for each colour band. Glacier extent data are sourced from the Global Land Ice Measurements from Space (GLIMS) database (Raup et al., 2007). (b) and (c) Geographic distribution of ~~CRN International~~ *CRN Global* basins with present-day glacier coverage, presented on two maps for visual clarity.

^{10}Be denudation rates represent end-member minimum values, and the differences from the uncorrected ^{10}Be denudation rates in the OCTOPUS database reflect end-member maximum values.

To our knowledge, corrections for glacier coverage in denudation rate calculations are rarely attempted in the literature, primarily because doing so accurately is impossible due to lack of relevant data. Nevertheless, the median difference between corrected and uncorrected ^{10}Be-derived denudation rates for basins with present-day ice occupying between $10-20\%$ of basin area ($n = 146$) may be as high as 24%, and for basins with $20-50\%$ glacier coverage ($n = 153$), may be as high as 46%, for example (Fig. 6), exceeding the uncertainties of the calculated denudation rates. While our calculations represent end-member values, they may still provide valuable insights into the potential influence of glaciers on the overestimation of ^{10}Be-derived denudation rates when no correction is applied. To this end, the updated *CRN* ~~International~~*Global* collection includes five additional data fields: `EBEGLA` and `EBEGLA_ERR`, which represent the glacier-corrected ^{10}Be denudation rates and associated uncertainties as calculated by CAIRN; `EBE_DIFF`, indicating the percentage difference between ^{10}Be denudation rates calculated without glacier correction and those adjusted for maximum present-day glacier impact; and `GLA_KM2` and `GLA_PCNT`, representing the areal extent of present-day glaciers in km^2 and percentage, respectively. All data and calculations are based on present-day glacier extents from the GLIMS database.

5 Limitations

The primary goal of the OCTOPUS project was to create a comprehensive database of cosmogenic nuclide-based denudation rates that is (1) globally consistent — achieved by recalculating all rates using a standardised methodology, and (2) reproducible

and reusable — made possible by providing all input geospatial data, extensive metadata, and by using open-source tools, such
195 as CAIRN. Adopting a global approach necessitates certain compromises. For instance, it requires selecting a DEM that is global or near global in extent and has a resolution suited to the range of basin areas included. Additionally, some corrections applied in individual studies — such as adjustments for quartz abundance variations or snow shielding — may be impractical for a global database due to a lack of consistent global data for these specific corrections.

While the absence of detailed meteorological data on snow thickness prevents us from evaluating the potential bias intro-
200 duced by omitting snow shielding corrections in our recalculated denudation rates, globally consistent, albeit low-resolution, lithological data are available. Although these data are insufficient for precise corrections related to quartz abundance, they may still be useful for assessing the overall quality of the recalculated data. To this end, *CRN ~~International~~Global* and *CRN Australia* include an additional field, labeled QTZ_PCNT, which indicates the percentage of basin area underlain by quartz-bearing rocks. This data was sourced from the Global Lithological Map (GLiM) by Hartmann and Moosdorf (2012). To identify the spatial
205 distribution of quartz-bearing rocks, we filtered the GLiM dataset by excluding specific lithological groups. Carbonate-rich sedimentary rocks and evaporites were removed, specifically those classified as carbonate sedimentary (sc), evaporite (ev), and also mixed sedimentary (sm) when the presence of carbonates was indicated. Additionally, we excluded groups classified as basic volcanic (vb) and basic plutonic (pb). Finally, metamorphic rocks (mt), with a secondary classification of mafic metamorphic (am), were also excluded. To reiterate, for most basins, these data are too coarse to enable precise corrections
210 to the recalculated denudation rates; however, they may still offer valuable insights and help identify basins where such corrections could be warranted. For example, in only $\sim 65\%$ ($n = 3,681$) of the basins in *CRN ~~International~~Global* and *CRN Australia*, quartz bearing rocks constitute more than 90% of the basin area. Quartz bearing rocks constitute less than half of the basin area in $\sim 15\%$ ($n = 869$) of basins, and less than 10% of basin area in $\sim 6\%$ ($n = 351$) of basins.

To maintain consistency with previous database versions, the ^{10}Be and ^{26}Al denudation rates in the *CRN ~~International~~Global*
215 and *CRN Australia* collections were corrected for topographic shielding using the method outlined in Codilean (2006). However, a recent study by DiBiase (2018) suggests that topographic shielding corrections are generally unnecessary for calculating basin-wide denudation rates, except in steep catchments where quartz distribution and / or denudation rates are not uniform. Nevertheless, the effect of topographic shielding corrections is minimal~~: omitting this correction in the basins with the 10% highest topographic shielding values ($n \approx 410$) only shifts denudation rates by 3.5% to 10% — a range within the~~. In the case
220 of ^{10}Be, for example, the median difference between denudation rates calculated with and without correcting for topographic shielding is only $\sim 1\%$ (IQR = 0.3 to 2.6%), and $\sim 99\%$ of the data have differences below the median uncertainty of the calculated ~~rates (see Codilean et al., 2022). As a result~~denudation rates. Thus, while disregarding topographic shielding ~~would yield~~yields slightly higher denudation rates, these differences ~~would~~ fall within the current uncertainty levels. ~~Therefore~~Given the computational cost, a recalculation of the *CRN ~~International~~Global* and *CRN Australia* collections without topographic
225 shielding correction using CAIRN is not justified~~given the computational cost~~. To address the issue of topographic shielding, however, and enable users to directly compare denudation rates with and without this correction, we include in *CRN Global* and *CRN Australia*, ^{10}Be and ^{26}Al denudation rates calculated using CENTR_LAT and ATM_PRESS with the LSDn scaling scheme in the Balco et al. (2008) calculator, both with and without correcting for topographic shielding.
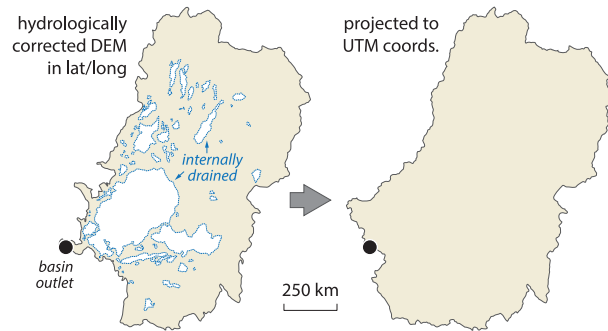
Figure 7. Drainage basin of the Murray-Darling river as derived from a hydrologically corrected DEM (left) versus that derived by CAIRN from the same DEM after projection to UTM coordinates (right). Note the absence of internally drained areas and the shifts in the location of the drainage divide following projection. See text for more details.

The CAIRN program requires input DEM data to be projected in one of the WGS84 UTM zones. This DEM is then used to derive a flow network, delineate individual basins, and link each grid cell within the basin to the sampling sites at the outlet. The requirement to project data into WGS84 UTM zones can pose challenges for large river basins that span multiple UTM zones. In such cases, the DEM must be projected into one of these zones, which increases distortion in the resulting DEM. Moreover, the requirement to project data introduces challenges in low-relief regions — such as the interior of the Australian continent (Tooth, 1999) — where internally drained areas within drainage basins are common. Projecting the data in such areas can artificially connect these internally drained sub-basins to the main drainage network. (Fig. 7). Fortunately, due to the subdued topography in these regions, any errors in the calculated basin-wide production rates are minimal. Nevertheless, basins with significant errors have been excluded from the database.

6 Conclusions

OCTOPUS v2.3 introduces ~~updated~~ updates to *CRN Denudation* ~~datasets~~, expanding the *CRN* ~~*International*~~ *Global* and *CRN Australia* collections with 1,311 additional river basins. These updates bring the total number of basins with recalculated ^{10}Be denudation rates to 5,611 and those with recalculated ^{26}Al rates to 561. Enhancements to data relevance and usability were achieved by removing redundant fields, ensuring that only essential information remains for each collection. New data fields now include the latitude of each basin's centroid and its effective basin-averaged atmospheric pressure, improving interoperability with online erosion rate calculators. Additional fields track the extent of present-day glaciers and their potential influence on denudation rates, along with estimates of quartz-bearing lithologies in each basin, providing a framework for evaluating data quality. We hope that the OCTOPUS database will continue to ensure data reusability well beyond the scope of their initial collection, thereby enabling large-scale, synoptic studies that would otherwise be unattainable.

Data availability. OCTOPUS v2.3 can be accessed at https://octopusdata.org (last access: 01 Feb 2025). The updated data collections have been assigned the following DOIs: 10.71747/uow-r3gk326m.28216865.v1 for *CRN Global* (Codilean and Munack, 2024a) and 10.71747/uow-r3gk326m.28216919.v1 for *CRN Australia* (Codilean and Munack, 2024b). Users should refer to the DOIs provided to ensure that they are accessing the current and supported version of the data. Comprehensive online documentation can be accessed at: https://octopus-db.github.io/documentation/ (last access: 01 Feb 2025). Supplementary data that was used in this paper but is not available via the OCTOPUS database, can be accessed at: https://doi.org/10.5281/zenodo.14014985 (Codilean and Munack, 2024c).

Author contributions. ATC and HM contributed equally to the work presented here.

Competing interests. The contact author has declared that neither they nor their co-author have any competing interests.

Acknowledgements. We acknowledge financial support from the Australian Research Council Centre of Excellence for Australian Biodiversity and Heritage (ARC Grant CE170100015). We thank Richard Ott, Greg Balco, and Roman DiBiase for careful reviews of the discussion paper. We also thank the cosmogenic nuclide community for generously sharing their data.

References

260   Balco, G.: Technical note: A prototype transparent-middle-layer data management and analysis infrastructure for cosmogenic-nuclide exposure dating, Geochronology, 2, 169–175, https://doi.org/10.5194/gchron-2-169-2020, 2020.

Balco, G., Stone, J. O., Lifton, N. A., and Dunai, T. J.: A complete and easily accessible means of calculating surface exposure ages or erosion rates from ^{10}Be and ^{26}Al measurements, Quaternary Geochronology, 3, 174–195, https://doi.org/10.1016/j.quageo.2007.12.001, 2008.

265   Charreau, J., Blard, P., Zumaque, J., Martin, L. C., Delobel, T., and Szafran, L.: Basinga: A cell-by-cell GIS toolbox for computing basin average scaling factors, cosmogenic production rates and denudation rates, Earth Surface Processes and Landforms, 44, 2349–2365, https://doi.org/10.1002/esp.4649, 2019.

Chen, Y., Wu, B., Xiong, Z., Zan, J., Zhang, B., Zhang, R., Xue, Y., Li, M., and Li, B.: Evolution of eastern Tibetan river systems is driven by the indentation of India, Communications Earth & Environment, 2, 256, https://doi.org/10.1038/s43247-021-00330-4, 2021.

270   Codilean, A., Fülöp, R.-H., Munack, H., Wilcken, K., Cohen, T., Rood, D., Fink, D., Bartley, R., Croke, J., and Fifield, L.: Controls on denudation along the East Australian continental margin, Earth-Science Reviews, 214, 103 543, https://doi.org/10.1016/j.earscirev.2021.103543, 2021.

Codilean, A. T.: Calculation of the cosmogenic nuclide production topographic shielding scaling factor for large areas using DEMs, Earth Surface Processes and Landforms, 31, 785–794, https://doi.org/10.1002/esp.1336, 2006.

275   Codilean, A. T. and Munack, H.: OCTOPUS Database v.2.3: The CRN Denudation Global collection [2024] [Data set], https://doi.org/10.71747/uow-r3gk326m.28216865.v1, 2024a.

Codilean, A. T. and Munack, H.: OCTOPUS Database v.2.3: The CRN Denudation Australian collection [2024] [Data set], https://doi.org/10.71747/uow-r3gk326m.28216919.v1, 2024b.

Codilean, A. T. and Munack, H.: Supplementary material for: Updated CRN Denudation collections in OCTOPUS v2.3 (Version 1) [Data
280   set], https://doi.org/10.5281/zenodo.14014985, 2024c.

Codilean, A. T., Munack, H., Cohen, T. J., Saktura, W. M., Gray, A., and Mudd, S. M.: OCTOPUS: an open cosmogenic isotope and luminescence database, Earth System Science Data, 10, 2123 – 2139, https://doi.org/10.5194/essd-10-2123-2018, 2018.

Codilean, A. T., Munack, H., Saktura, W. M., Cohen, T. J., Jacobs, Z., Ulm, S., Hesse, P. P., Heyman, J., Peters, K. J., Williams, A. N., Saktura, R. B. K., Rui, X., Chishiro-Dennelly, K., and Panta, A.: OCTOPUS database (v.2), Earth System Science Data, 14, 3695–3713,
285   https://doi.org/10.5194/essd-14-3695-2022, 2022.

Compo, G. P., Whitaker, J. S., Sardeshmukh, P. D., Matsui, N., Allan, R. J., Yin, X., Gleason, B. E., Vose, R. S., Rutledge, G., Bessemoulin, P., Brönnimann, S., Brunet, M., Crouthamel, R. I., Grant, A. N., Groisman, P. Y., Jones, P. D., Kruk, M. C., Kruger, A. C., Marshall, G. J., Maugeri, M., Mok, H. Y., Nordli, O., Ross, T. F., Trigo, R. M., Wang, X. L., Woodruff, S. D., and Worley, S. J.: The Twentieth Century Reanalysis Project, Quarterly Journal of the Royal Meteorological Society, 137, 1–28, https://doi.org/10.1002/qj.776, 2011.

290   Delunel, R., Schlunegger, F., Valla, P. G., Dixon, J., Glotzbach, C., Hippe, K., Kober, F., Molliex, S., Norton, K. P., Salcher, B., Wittmann, H., Akçar, N., and Christl, M.: Late-Pleistocene catchment-wide denudation patterns across the European Alps, Earth-Science Reviews, 211, 103 407, https://doi.org/10.1016/j.earscirev.2020.103407, 2020.

DiBiase, R. A.: Short Communication: Increasing vertical attenuation length of cosmogenic nuclide production on steep slopes negates topographic shielding corrections for catchment erosion rates, Earth Surface Dynamics, 6, 923–931, https://doi.org/10.5194/esurf-6-923-
295   2018, 2018.

Godard, V. and Tucker, G. E.: Influence of Climate-Forcing Frequency on Hillslope Response, Geophysical Research Letters, 48, e2021GL094 305, https://doi.org/10.1029/2021gl094305, 2021.

Halsted, C., Bierman, P., Codilean, A., Corbett, L., and Caffee, M.: Global analysis of in situ cosmogenic ^{26}Al/^{10}Be ratios in fluvial sediments indicates widespread sediment storage and burial during transport, Geochronology Discussions, pp. 1–19, https://doi.org/10.5194/gchron-2024-22, 2024.

Hartmann, J. and Moosdorf, N.: The new global lithological map database GLiM: A representation of rock properties at the Earth surface, Geochemistry, Geophysics, Geosystems, 13, Q12 004, https://doi.org/10.1029/2012gc004370, 2012.

Herbert, A. V., Haberle, S. G., Flantua, S. G. A., Mottl, O., Blois, J. L., Williams, J. W., George, A., and Hope, G. S.: The Indo-Pacific Pollen Database — a Neotoma constituent database, Climate of the Past, 20, 2473–2485, https://doi.org/10.5194/cp-20-2473-2024, 2024.

Lifton, N., Sato, T., and Dunai, T. J.: Scaling in situ cosmogenic nuclide production rates using analytical approximations to atmospheric cosmic-ray fluxes, Earth and Planetary Science Letters, 386, 149 – 160, https://doi.org/10.1016/j.epsl.2013.10.052, 2014.

Marrero, S. M., Phillips, F. M., Borchers, B., Lifton, N., Aumer, R., and Balco, G.: Cosmogenic nuclide systematics and the CRONUScalc program, Quaternary Geochronology, 31, 160 – 187, https://doi.org/10.1016/j.quageo.2015.09.005, 2016.

Mudd, S. M., Harel, M.-A., Hurst, M. D., Grieve, S. W. D., and Marrero, S. M.: The CAIRN method: automated, reproducible calculation of catchment-averaged denudation rates from cosmogenic nuclide concentrations, Earth Surface Dynamics, 4, 655–674, https://doi.org/10.5194/esurf-4-655-2016, 2016.

Mudd, S. M., Clubb, F. J., Grieve, S. W. D., Milodowski, D. T., Gailleton, B., Hurst, M. D., Valters, D. V., Wickert, A. D., and Hutton, E. W. H.: LSDtopotools/LSDTopoTools2: LSDTopoTools2 v0.9, https://doi.org/10.5281/zenodo.8076231, 2023.

Nishiizumi, K.: Preparation of ^{26}Al AMS standards, Nuclear Instruments and Methods in Physics Research Section B: Beam Interactions with Materials and Atoms, 223, 388 – 392, https://doi.org/10.1016/j.nimb.2004.04.075, 2004.

Nishiizumi, K., Winterer, E. L., Kohl, C. P., Klein, J., Middleton, R., Lal, D., and Arnold, J. R.: Cosmic ray production rates of ^{10}Be and ^{26}Al in quartz from glacially polished rocks, Journal of Geophysical Research: Solid Earth, 94, 17 907–17 915, https://doi.org/10.1029/jb094ib12p17907, 1989.

Nishiizumi, K., Imamura, M., Caffee, M. W., Southon, J. R., Finkel, R. C., and McAninch, J.: Absolute calibration of ^{10}Be AMS standards, Nuclear Instruments and Methods in Physics Research Section B: Beam Interactions with Materials and Atoms, 258, 403 – 413, https://doi.org/10.1016/j.nimb.2007.01.297, 2007.

Peters, K. J., Saltré, F., Friedrich, T., Jacobs, Z., Wood, R., McDowell, M., Ulm, S., and Bradshaw, C. J. A.: FosSahul 2.0, an updated database for the Late Quaternary fossil records of Sahul, Scientific Data, 6, 272, https://doi.org/10.1038/s41597-019-0267-3, 2019.

Peters, K. J., Saltré, F., Friedrich, T., Jacobs, Z., Wood, R., McDowell, M., Ulm, S., and Bradshaw, C. J. A.: Addendum: FosSahul 2.0, an updated database for the Late Quaternary fossil records of Sahul, Scientific Data, 8, 133, https://doi.org/10.1038/s41597-021-00918-7, 2021.

Phillips, F. M., Argento, D. C., Balco, G., Caffee, M. W., Clem, J., Dunai, T. J., Finkel, R., Goehring, B., Gosse, J. C., Hudson, A. M., Jull, A. T., Kelly, M. A., Kurz, M., Lal, D., Lifton, N., Marrero, S. M., Nishiizumi, K., Reedy, R. C., Schaefer, J., Stone, J. O., Swanson, T., and Zreda, M. G.: The CRONUS-Earth Project: A synthesis, Quaternary Geochronology, 31, 119–154, https://doi.org/10.1016/j.quageo.2015.09.006, 2016.

Raup, B., Racoviteanu, A., Khalsa, S. J. S., Helm, C., Armstrong, R., and Arnaud, Y.: The GLIMS geospatial glacier database: A new tool for studying glacier change, Global and Planetary Change, 56, 101–110, https://doi.org/10.1016/j.gloplacha.2006.07.018, 2007.

Rehn, E., Cadd, H., Mooney, S., Cohen, T. J., Munack, H., Codilean, A. T., Adeleye, M., Beck, K. K., IV, M. C., Gouramanis, C., Hanson, J. M., Jones, P. J., Kershaw, A. P., Mackenzie, L., Maisie, M., Mariani, M., Mately, K., McWethy, D., Mills, K., Moss, P., Patton, N. R.,

335  Rowe, C., Stevenson, J., Tibby, J., and Wilmshurst, J.: The SahulCHAR Collection: A Palaeofire Database for Australia, New Guinea, and New Zealand, Earth System Science Data Discussions, 2024, 1–20, https://doi.org/10.5194/essd-2024-328, 2024.

Saktura, W. M., Rehn, E., Linnenlucke, L., Munack, H., Wood, R., Petchey, F., Codilean, A. T., Jacobs, Z., Cohen, T. J., Williams, A. N., and Ulm, S.: SahulArch: A geochronological database for the archaeology of Sahul, Australian Archaeology, 89, 1–13, https://doi.org/10.1080/03122417.2022.2159751, 2023.

340 Schaefer, J. M., Codilean, A. T., Willenbring, J. K., Lu, Z.-T., Keisling, B., Fülöp, R.-H., and Val, P.: Cosmogenic nuclide techniques, Nature Reviews Methods Primers, 2, 1–22, https://doi.org/10.1038/s43586-022-00096-9, 2022.

Sternai, P., Sue, C., Husson, L., Serpelloni, E., Becker, T. W., Willett, S. D., Faccenna, C., Giulio, A. D., Spada, G., Jolivet, L., Valla, P., Petit, C., Nocquet, J.-M., Walpersdorf, A., and Castelltort, S.: Present-day uplift of the European Alps: Evaluating mechanisms and models of their relative contributions, Earth-Science Reviews, 190, 589–604, https://doi.org/10.1016/j.earscirev.2019.01.005, 2019.

345 Stone, J. O.: Air pressure and cosmogenic isotope production, Journal of Geophysical Research: Solid Earth, 105, 23 753–23 759, https://doi.org/10.1029/2000JB900181, 2000.

Stübner, K., Balco, G., and Schmeisser, N.: RIVERSAND: A new tool for efficient computation of catchmentwide erosion rates, Radiocarbon, pp. 1–14, https://doi.org/10.1017/rdc.2023.74, 2023.

Tooth, S. D.: Floodouts in Central Australia, in: Varieties of Fluvial Form, edited by Miller, A. J. and Gupta, A., pp. 219–247, Wiley & Sons,

350 Chichester, 1999.

Whipple, K., Adams, B., Forte, A., and Hodges, K.: Eroding the Himalaya: Topographic and Climatic Control of Erosion Rates and Implications for Tectonics, The Journal of Geology, 131, 265–288, https://doi.org/10.1086/731260, 2023.

Wilner, J. A., Nordin, B. J., Getraer, A., Gregoire, R. M., Krishna, M., Li, J., Pickell, D. J., Rogers, E. R., McDannell, K. T., Palucis, M. C., and Keller, C. B.: Limits to timescale dependence in erosion rates: Quantifying glacial and fluvial erosion across timescales, Science

355 Advances, 10, eadr2009, https://doi.org/10.1126/sciadv.adr2009, 2024.

Zondervan, J. R., Hilton, R. G., Dellinger, M., Clubb, F. J., Roylands, T., and Ogrič, M.: Rock organic carbon oxidation CO_2 release offsets silicate weathering sink, Nature, pp. 1–5, https://doi.org/10.1038/s41586-023-06581-9, 2023.